JCI insight

IRF5 governs macrophage adventitial infiltration to fuel abdominal aortic aneurysm formation

Yidong Wang, … , Zhejun Cai, Meixiang Xiang

JCI Insight. 2024. https://doi.org/10.1172/jci.insight.171488.

Research In-Press Preview **Vascular biology**

Graphical abstract

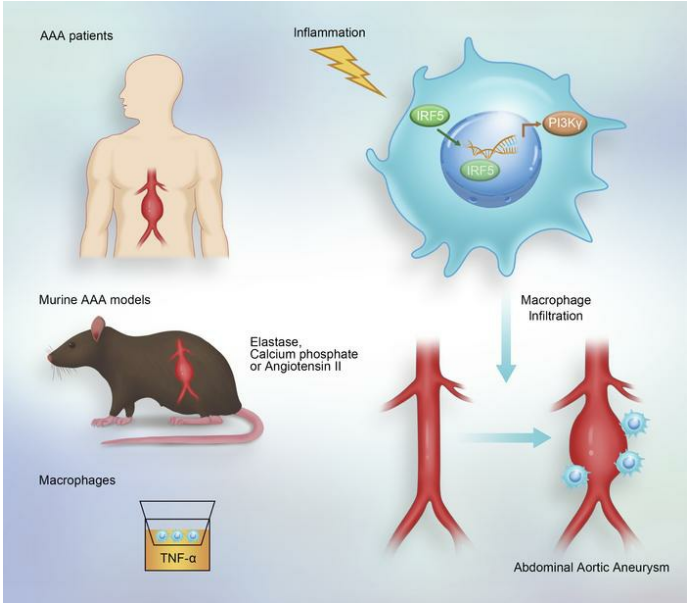

IRF5 governs macrophage adventitial infiltration to fuel abdominal aortic aneurysm formation

Yidong Wang[1]; Zhenjie Liu[2];Shen Song[3]; Jianfang Wang[1]; Chunna Jin[1]; Liangliang Jia[1]; Yuankun Ma[1]; Tan Yuan[1]; Zhejun Cai[1]; Meixiang Xiang[1]

1.Department of Cardiology, State Key Laboratory of Transvascular Implantation Devices, Provincial Key Laboratory of Cardiovascular Research, The Second Affliated Hospital Zhejiang University School of Medicine, 88 Jiefang Rd, Hangzhou 310009, P.R. China

2.Department of Vascular Surgery, The second Affiliated Hospital of Zhejiang University School of Medicine, 88 Jiefang Rd, Hangzhou 310009, P.R. China

3.State Key Laboratory of Cardiovascular Disease, Fuwai Hospital, National Center for Cardiovascular Disease, Chinese Academy of Medical Sciences and Peking Union Medical College, Beijing, China

Conflict of interest: The authors have declared that no conflict of interest exists.

Authorship note: YW and ZL contributed equally to the work.

Correspondence to Meixiang Xiang or Zhejun Cai. Department of Cardiology, The Second Affliated Hospital, Zhejiang University School of Medicine, 88 Jiefang Rd, Hangzhou, Zhejiang 310009, China. E-mails: xiangmx@zju.edu.cn; caizhejun@zju.edu.cn.

Abstract

Abdominal aortic aneurysm (AAA) is a chronic inflammatory disease characterized by the expansion of the aortic wall. One of the most significant features is the infiltration of macrophages in the adventitia, which drives vasculature remodeling. The macrophage-derived interferon regulatory factor 5 (IRF5) in macrophage infiltration and AAA formation remains unknown. RNA sequencing of AAA adventitia identifies *Irf5* as the top significantly increased transcriptional factor, which is predominantly expressed in macrophages. Global and myeloid specific deficiency of *Irf5* reduces AAA progression, with marked reduction of macrophage infiltration. Further cellular investigations indicate that IRF5 promotes macrophage migration by direct regulation of downstream phosphoinositide 3-kinase gamma (PI3Kγ, *Pik3cg*). *Pik3cg* ablation hinders AAA progression, and myeloid-specific salvage of *Pik3cg* restores AAA progression and macrophage infiltration derived from *Irf5* deficiency. Finally, we discovered that the IRF5 and PI3Kγ expression in the adventitia are significantly increased in AAA patients. These findings uncover that the IRF5-dependent regulation of PI3Kγ is essential for AAA formation.

Key Words: Abdominal aortic aneurysm; IRF5; macrophage; migration; PI3Kγ

Non-standard Abbreviations and Acronyms

AAA	abdominal aortic aneurysm (AAA)
IRF5	interferon regulatory factor 5
PI3Kγ	phosphoinositide 3-kinase gamma
MMPs	matrix metalloproteinases
IRFs	interferon regulatory factors
TLRs	toll-like receptors
RNA-seq	RNA sequencing
GO	Gene Ontology
WT	wild type
$CaPO_4$	calcium phosphate
BMDMs	bone marrow-derived macrophages
DEGs	differentially expressed genes

INTRODUCTION

Abdominal aortic aneurysm (AAA) is characterized by progressive abdominal aortic dilation exceeding the normal diameter by more than 50%(1). The most catastrophic clinical consequence of AAA progression is acute rupture, which carries a mortality of 80%(2,3). However, no effective pharmacological therapy for AAA is available so far(4). Vasculature inflammation is an essential hallmark for AAA formation. A variety of inflammatory cells are trapped in the adventitia of aneurysmal tissues, which contribute to adventitial remodeling and AAA development(5-7), whereas macrophages are mainstays in the inflammatory microenvironment. Macrophages are continuously recruited and activated in the adventitia in this inflammation state, producing matrix metalloproteinases (MMPs) and pro-inflammatory cytokines, which exacerbate aortic expansion(5). Although increased inflammation and macrophage infiltration in AAA are well documented, the molecular basis of how macrophages are infiltrated and activated remain poorly characterized.

Interferon regulatory factors (IRFs) are a family of nine transcription factors (IRF1-9) involved in cytosolic pattern recognition receptor- and toll-like receptors (TLRs)-mediated signal transduction and immune cell differentiation(8). Among them, IRF5 is a crucial regulator of macrophages function(8). It mediates the development of various inflammatory diseases. However, whether IRF5 is involved in AAA remains unclear.

Here we reveal that IRF5 is the top significantly upregulated transcriptional

factor in the adventitia of AAA, which is predominantly expressed in infiltrated macrophages. We demonstrate that IRF5 mediates macrophages infiltration to drive AAA progression. Mechanistically, IRF5 transcriptionally activates *Pik3cg*, which is known to have a crucial role in macrophage migration. Thus, IRF5 is critical in adventitial macrophage recruitment and AAA development.

RESULTS

Identification of IRF5 as a potential determinant of adventitial inflammation in AAA

Adventitial inflammation, characterized by continuous recruitment of inflammatory cells, notably contributed to adventitial remodeling and AAA progression(9,10). We first harvested the adventitia of elastase-induced AAA samples and the controls to perform RNA sequencing (RNA-seq). Extensive inflammation was present in the adventitia. The enrichment analysis showed dramatically enhanced upregulation of various genes and pathways, including immune cell activation and migration (Supplemental Figure 1A and 1B).

Notably, *Irf5* expression showed the most significant alteration among transcriptional factors between AAA and the controls (Supplemental Figure 1C). Interestingly, the gene expression of another two IRF family members, *Irf7* and *Irf8,* were also ranked among the top 5 of the most significantly upregulated genes (Supplemental Figure 1C). We analyzed the cell-specific expression of *Irf5* in the single-cell RNA-seq of the elastase-induced AAA tissue from the dataset provided by Zhao et al(11). *Irf5*, not other transcriptional factors, was highly expressed in macrophages subsets (Supplemental Figure 2, Supplemental Figure 3).

We next investigated the protein changes of IRF5 in elastase and calcium phosphate ($CaPO_4$)-induced murine AAA tissues. Macrophages were considerably infiltrated as expected. In the normal abdominal aorta, IRF5 was

hardly observed. However, IRF5 was highly expressed in AAA tissues, induced by elastase and $CaPO_4$(Figure 1A through 1D, Supplemental Figure 4). Dual immunofluorescence staining further revealed that IRF5 was mostly colocalized with CD68, the macrophage marker, which is consistent with our preliminary bioinformatic analysis, that IRF5 is predominantly expressed in macrophages in AAA (Figure 1A through 1C, Supplemental Figure 4A through 4C).

Deficiency of *Irf5* attenuates AAA formation in vivo

Our findings implicated the potential involvement of IRF5 in AAA development. We next to determine whether *Irf5* ablation may alter AAA development in vivo. 10- to 12- week-old male C57BL/6 mice genetical ablation of *Irf5* and wild type (WT) littermates were subjected to elastase-induced AAA. After 14 days, the abdominal aorta perfused with elastase revealed a significant increase in aortic diameter, compared to those treated with inactive elastase (Supplemental Figure 5A). Mice with *Irf5* deficiency showed reduced aortic dilation, treated with elastase or $CaPO_4$ (Supplemental Figure 5A through 5D). These data emphasized the vital role of IRF5 in AAA development.

Because IRF5 is mainly located in macrophages, we sought to determine the action of *Irf5* in myeloid cells in AAA development. We generated the myeloid cell-specific *Irf5* deficient mice ($Irf5^{\Delta M\Phi}$) by crossing $Irf5^{flox/flox}$ with $Lyz2^{Cre}$ mice. In consistent to the results from *Irf5* deficiency mice, AAA

progression induced by elastase perfusion or $CaPO_4$ treatment for two weeks was also delayed in *Irf5*$^{\Delta M\Phi}$ mice, compared with the littermate *Irf5*$^{flox/flox}$ mice (Figure 2A and 2B, Supplemental Figure 6A and 6B). Van Gieson staining was conducted in *Irf5*$^{flox/flox}$ and *Irf5*$^{\Delta M\Phi}$ mice subjected to elastase, demonstrating that severity of elastin degradation, measured by elastin degradation scores, was alleviated in aneurysmal tissues harvested from *Irf5*$^{\Delta M\Phi}$ mice(Supplemental Figure 7A). Reduction of MMP-9 was also observed in tissues from *Irf5*$^{\Delta M\Phi}$ mice, with preserved MMP-2 expression(Supplemental Figure 7B and 7C). Moreover, infiltration of other inflammatory cells, such as T cells, dendritic cells and neutrophils, was detected. Immunoflurescence results concluded that CD3 and MHC-II, markers of T cells and dendritic cells, were hardly observed in AAA of *Irf5*$^{flox/flox}$ and *Irf5*$^{\Delta M\Phi}$ mice, while Ly6G, respresenting neutrophils, was slightly decreased in *Irf5*$^{\Delta M\Phi}$ mice(Supplemental Figure 8A and 8B) Angiotensin-II (Ang-II) infusion in apolipoprotein E deficient (*Apoe*$^{-/-}$) mice is another common AAA model(12,13). To further validate the effect of myeloid *Irf5* in AAA development, *Apoe*$^{-/-}$ *Irf5*$^{flox/flox}$ and *Apoe*$^{-/-}$ *Irf5*$^{\Delta M\Phi}$ mice were generated and infused with Ang-II for 28 days. Consistently, the aortic dilation in *Apoe*$^{-/-}$ *Irf5*$^{\Delta M\Phi}$ mice were less than that in *Apoe*$^{-/-}$ *Irf5*$^{flox/flox}$ mice (Supplemental Figure 9A through 9B). 5 mice, of 23, were died with rupture in *Apoe*$^{-/-}$ *Irf5*$^{flox/flox}$ group, while only 2 mice were died in the population of 21 mice in *Apoe*$^{-/-}$ *Irf5*$^{\Delta M\Phi}$ group(Supplemental Figure 9C). Additionally, macrophage infiltration was also reduced in *Apoe*$^{-/-}$ *Irf5*$^{\Delta M\Phi}$ mice

(Supplemental Figure 9D).

To further rule out the possible effects of IRF5 ablation in other myeloid-derived cells on AAA progression, adoptive monocyte transfer was performed(14). Mice with *Irf5* deletion were subjected to elastase treatment and subsequently intravenously injected with PKH26 pre-stained monocytes isolated from mice with wild type (WT to KO) or *Irf5* loss (KO to KO), respectively. Immunofluorescence staining demonstrated that more PKH26 positive macrophages were infiltrated in aortas from WT to KO mice than KO to KO mice (Supplemental Figure 10A and 10B). Besides, WT to KO mice showed a larger abdominal aortic diameter than KO to KO mice (Supplemental Figure 10C and 10D). These results supported that *Irf5* deficiency in monocytes (macrophages), not other cells, attenuated AAA progression.

IRF5 drives macrophages infiltration

Previous investigations suggest that transmural macrophage migration potentiates AAA, and defective migration ability of macrophage mitigates AAA(15-17). Considering the RNA-seq data that migration-associated genes were upregulated in the adventitia of AAA (Supplemental Figure 1A and 1B), we sought to investigate whether IRF5 may alter macrophages infiltration.

Compared to the control mice, myeloid-specific *Irf5* deficiency mice challenged with elastase perfusion-induced AAA resulted in a marked reduction of macrophages infiltration detected by CD68 immunofluorescence

staining and flow cytometry (Figure 2C through 2E). We conducted RNA-seq of AAA tissues of from wild type mice and *Irf5*$^{-/-}$ mice, and the results showed that migration related genes were significantly decreased (Figure 3A and 3B). In addition, RNA-seq revealed that compared to control bone marrow-derived macrophages (BMDMs), migration related genes in *Irf5*-silenced BMDMs treated with TNF-α were also dramatically altered (Supplemental Figure 11A and 11B). These data confirmed that IRF5 is correlated with macrophage migration.

We further investigated the BMDMs migration ability stimulated by TNF-α from *Irf5*$^{flox/flox}$ and *Irf5*$^{\Delta M\Phi}$ mice. The wound healing assays suggested that macrophages with *Irf5* deficiency showed a halted migration into the wound zone, compared with control macrophages (Figure 3C). The transwell migration assays were further conducted. BMDMs were seeded in the upper chamber, and a medium with TNF-α was placed in the lower chamber. The numbers of *Irf5* deficient BMDMs migrated to the lower surface of inserts were reduced (Figure 3D).

Additionally, We observed that myeloid *Irf5* ablation did not disrupt macrophage proliferation, as reflected by the expression of proliferating cell nuclear antigen (PCNA) in BMDMs(Supplemental Figure 12A and 12B). The numbers of monocytes in peripheral blood from *Irf5*$^{flox/flox}$ and *Irf5*$^{\Delta M\Phi}$ mice were also similar (Supplemental Figure 13). The data rule out the possibility that IRF5 increased the numbers of infiltrated macrophages by enhancing

proliferation or migration out of the bone marrow. Nevertheless, *Irf5* deficiency moderately decreased IL-1β and IL-6, and increased phagocytosis related genes, CD36 and Itgb3, in BMDMs(Supplemental Figure 14). These data suggested the multifunction of IRF5 in regulation of AAA development.

IRF5 contributes to macrophage migration *via* PI3Kγ

Since IRF5 is a transcriptional factor and is expressed explicitly in macrophages, we managed to find which migration related genes altered by IRF5 may serve as downstream transcriptional regulated targets in macrophages. Overlapping differentially expressed genes (DEGs), migration related genes, macrophage highly expressed genes, and genes with potential IRF5 binding site, we found 15 genes (Figure 4A and 4B). Among them, *Pik3cg* highly expressed in macrophages of AAA, is a potent regulator of macrophage migration, while previous research indicated that inhibition of PI3Kγ reduced AAA development(Supplemental Figure 15A through 15F)(18). Additionally, *Pik3cg* was also down-regulated in si-*irf5* BMDMs treated with TNF-α (Supplemental Figure 11B). These all implied that *Pik3cg* is a potentially important downstream candidate of IRF5. We validated the gene changes by qPCR and western blot. Under TNF-α stimulation, IRF5 and PI3Kγ were simultaneously increased in WT BMDMs, both in mRNA and protein levels (Figure 4C and 4D). However, the TNF-α-induced PI3Kγ expression was significantly decreased in *Irf5* deficient BMDMs (Figure 4C and 4D).

We investigated whether IRF5 specially binds to the *Pik3cg* gene promoter in BMDMs by chromatin immunoprecipitation assay. In BMDMs, the *Pik3cg* gene promoter was positively amplified in samples from TNF-α-treated cells following immunoprecipitation with IRF5 antibody but not with control IgG, suggesting that the positive amplification of the *Pik3cg* gene promoter is specific to IRF5 (Figure 4E). Dual-luciferase assay further demonstrated that IRF5 plasmids significantly promoted the *Pik3cg* transcriptional activity in HEK 293T cells (Figure 4F). This effect could be hindered by the mutation of the IRF5-binding motif (-1060 to -1047) (Figure 4F).

We next determined whether IRF5-mediated macrophage migration is PI3Kγ dependent. *Pik3cg* (*H11-CAG-LSL-Pik3cg-Flag-polyA*) was knocked into the *Irf5*$^{\Delta M\Phi}$ mice to generate the *Flag-Pik3cg*$^{Tg/+}$*Irf5*$^{flox/flox}$*Lyz2*^{Cre} mice (*Pik3cg*$^{M\Phi+}$*Irf5*$^{\Delta M\Phi}$), of which *Pik3cg* was overexpressed in *Irf5* deficient myeloid cells. The efficacy of PI3Kγ overexpression in BMDMs was verified by western blot (Supplemental Figure 16A). As depicted in Figure 4G and 4H, overexpression of *Pik3cg* in *Irf5* deficient BMDMs increased the migration ability compared to the *Irf5* deficient controls. The data provide evidence that IRF5-regulated macrophage migration is *via* PI3Kγ.

PI3Kγ is required for AAA development

Direct evidence of PI3Kγ in the development of AAA is still lacking. PI3Kγ was upregulated in elastase-induced AAA aortas, mainly colocalized with CD68

positive macrophages, not in endothelial cells or vascular smooth muscle cells (Figure 5A through 5C, Supplemental Figure 15E and 15F). We examined the effect of *Pik3cg* deficiency on elastase or $CaPO_4$-induced AAA. Deficiency of *Pik3cg* led to a significant reduction of abdominal aortic enlargement (Figure 5D, Supplemental Figure 17). We also observed that *Pik3cg* ablation profoundly abolished the macrophages infiltration in the aortas (Figure 5F). The results implied that PI3Kγ promoted progression of AAA, partially relying on modulation of macrophage migration.

The effect of IRF5 on AAA formation is PI3Kγ dependent

Our data suggested the role of IRF5 and PI3Kγ in macrophages infiltration and AAA development. Based on the results that PI3Kγ mediates IRF5 regulation of macrophages migration, we speculated that PI3Kγ is crucial for IRF5-dependent AAA development.

The immunofluorescence staining showed that IRF5 and PI3Kγ were colocalized in the infiltrated macrophages of elastase-induced AAA (Supplemental Figure 18). The $Irf5^{flox/flox}$, $Irf5^{\Delta M\Phi}$, and $Pik3cg^{M\Phi+}Irf5^{\Delta M\Phi}$ mice were subjected to elastase or $CaPO_4$-induced AAA. The in vivo efficacy of PI3Kγ overexpression in macrophages was verified by staining PI3Kγ, FLAG, and CD68 (Supplemental Figure 16B through 16E). Our investigation revealed that upon elastase administration, myeloid cell-specific overexpression of *Pik3cg* restored abdominal aorta diameters increase compared to the $Irf5^{\Delta M\Phi}$

mice (Figure 6A and 6B). Similar results were also observed in *Irf5*$^{flox/flox}$, *Irf5*$^{\Delta M\Phi}$, and *Pik3cg*$^{M\Phi+}$*Irf5*$^{\Delta M\Phi}$ mice treated with $CaPO_4$ (Supplemental Figure 19). The *Pik3cg*$^{M\Phi+}$*Irf5*$^{\Delta M\Phi}$ mice increased macrophage infiltration compared to the *Irf5*$^{\Delta M\Phi}$ mice in elastase-perfused mice (Figure 6C through 6E).

IRF5 and PI3Kγ are increased in human AAA

Our data demonstrate that myeloid-derived IRF5 contributes to macrophage migration, aggravates elastase and $CaPO_4$-induced murine AAA via PI3Kγ. To confirm whether IRF5 and PI3Kγ were present in human AAA, immunofluorescence staining was conducted. Demographic characteristics of AAA patients were shown in Supplemental Table I. The results suggested that IRF5 expression was hardly detected in normal aortas but was dramatically elevated in macrophages of human AAA samples (Figure 7A through 7C). Consistently, PI3Kγ was also significantly upregulated in human AAA samples, which was mainly expressed in infiltrated macrophages (Figure 7D through 7F).

DISCUSSION

Adventitial macrophages are the major contributors to the development of AAA(5,10). Our study discovered, for the first time, that IRF5 was significantly increased in macrophages from adventitia of AAA. Myeloid-specific *Irf5* deletion attenuated AAA progression, with a reduction of macrophage

infiltration. Mechanistically, *Pik3cg* was identified as the downstream target and mediated the effects of *Irf5* on macrophage migration in vitro. *Pik3cg* ablation verified to reduce AAA expansion, and excessive PI3Kγ in macrophages facilitated AAA development (Supplemental Figure 20).

Adventitia is the most complex part of vascular walls. It consists of fibroblasts, immune cells, progenitor cells, and vasa vasorum endothelial cells(5,10). Traditionally, vascular inflammation has been regarded as an inside-out response, which illustrates that inflammatory cells are recruited in the intima and transmigrate to media and adventitia(10). Nevertheless, emerging evidence support the outside-in hypothesis, in which chronic vascular inflammation is initiated and maintained in the adventitia and subsequently affects media and intima(10). Robust inflammation is observed in the adventitia of elastase-induced AAA, confirmed by our RNA-seq data. Pathways associated with immune cell activation, proliferation, and migration are significantly upregulated, and many of these pathways are involved in macrophages. In AAA tissues, accumulated macrophages are mainly stemmed from bone marrow-derived monocytes(5). Reduced macrophage migration and infiltration have been proved to hamper AAA dilation(16,17). Nevertheless, updated studies point out that resident macrophages are also observed in the normal artery, and this population is from $CX3CR1^{+}$ precursors during the embryonic stage and bone-marrow-derived monocytes after birth(19). It is still unclear whether resident macrophages also contribute to the

pathogenesis of AAA since previous studies mainly focus on the roles of bone marrow-derived macrophages in AAA.

IRF5 drives macrophages to inflammatory responses and is involved in the pathogenesis of a variety of inflammatory diseases(20-22). IRF5 is activated by multiple TLRs and MyD88 pathway and translocated to nuclear to promote transcription of diverse pro-inflammatory cytokines(23,24). Traditionally, IRF5 is regarded as a regulator of macrophage polarization and can be used as a marker of inflammatory macrophages(20). Recently, a body of investigations demonstrates that the effects of IRF5 on macrophages are versatile. In adipose-tissue macrophages, deletion of *Irf5* facilitated TGF-β expression and enhanced collagen accumulation in adipose tissues(21). IRF5 in macrophages directly regulates CD11c to impair efferocytosis and consequently worsen the atherosclerosis(25,26). In adipose tissue macrophages, IRF5 is correlated with elevated oxidative respiration and mitochondrial membrane potential by regulating GHITM(27). Considering the critical role of IRF5 in inflammatory diseases, it is reasonable that IRF5 may participate in AAA development. Indeed, our data provide evidence of the crucial role of IRF5 in AAA progression. First, RNA-seq results show that *Irf5* is the top significantly increased transcriptional factor in the adventitia. Second, IRF5 is markedly increased in the infiltrated macrophages in the adventitia of AAA. Finally, myeloid cell-specific deletion of *Irf5* attenuates murine AAA development. The next exciting finding is the relationship between IRF5 and

366 macrophage migration. Despite the various reported mechanisms of IRF5 in
367 other inflammatory diseases(23), the same feature is, ablation of IRF5 reduces
368 the number of macrophages in these disease conditions. Our observations
369 identify that IRF5 ablation dramatically reduces macrophage numbers in AAA,
370 and we further rule out the ability of IRF5 in regulating macrophage
371 proliferation. Another possibility of how IRF5 ablation hampers tissue
372 macrophage numbers is that it may affect macrophage maturation. However,
373 previous reports have already demonstrated that IRF5 does not affect the
374 bone marrow and monocytes mobilization into circulation and
375 differentiation(28). The only left explanation is that IRF5 drives macrophages
376 migration. Our cellular investigations prove that IRF5 intrinsically regulates
377 macrophage migration, and RNA-seq analysis infers that IRF5 is pronouncedly
378 correlated with genes associated with cellular motility, independent of
379 alterations of chemokines and their receptors. In mechanism, PI3Kγ is the
380 direct downstream target of IRF5, which fuels macrophages migration.

381 PI3Kγ, mainly distributed in macrophages, is classically viewed as a
382 master regulator of migration(29,30). The mechanisms include the modulation
383 of selectin, integrin, and vimentin-dependent cytoskeleton organization(30,31).
384 In the diverse vascular diseases abovementioned, it is observed that PI3Kγ
385 deletion reduced infiltration immune cells(32,33). Administration of PI3Kγ
386 inhibitor, AS605240, significantly reduced atherosclerosis(32). Bone marrow
387 transplantation from *Pik3cg*$^{-/-}$ to *Ldlr*$^{-/-}$ alleviates atherosclerosis with

388 decreased macrophage infiltration(32). Genetic and pharmacological ablation
389 of PI3Kγ activity decreases arterial stenosis and macrophage aggregation(34).
390 Our experimental data further indicate that PI3Kγ is highly expressed in the
391 macrophages of AAA, and genetic ablation of *Pik3cg* inhibits AAA development
392 in vivo. Conversely, myeloid cell-specific overexpression of *Pik3cg* rescued *Irf5*
393 ablation-induced AAA reduction.

394 However, there are several limitations in this study. As reported
395 previously, IRF5 exerted pleiotropic effects on macrophage function including
396 macrophage polarization, efferocytosis and cytokine expression(20,21,25).
397 Further, our observations validated that *Irf5* deficiency disturbed cytokines and
398 phagocytosis related genes. MMP-9 was also showed a reduction in
399 accordance with previous study in myocardial infarction(35). Though our data
400 suggested that IRF5 regulated macrophage migration dependent on PI3Kγ,
401 other mechanisms may also involve in the AAA progression and can not
402 throughly excluded. Another limitation was that *Irf5* was inevitably ablated in
403 other myeloid cells such as dendritic cells and neutrophils in $Irf5^{\Delta M\Phi}$ mice,
404 compared to $Irf5^{flox/flox}$ mice. Infiltration of neutrophils was also reduced in
405 aneurysmal tissues $Irf5^{\Delta M\Phi}$ mice. $Irf5^{flox/flox}$ mice were used as controls
406 according to previous studies(36). Although an adoptive monocyte transfer
407 experiment was performed to validate the function of macrophage-derived
408 IRF5 in AAA progression, the exact roles of IRF5 in other myeloid cells like
409 dendritic cells and neutrophils in AAA require to be explored in the future.

In summary, we have established a crucial role of IRF5 in the pathogenesis of AAA. IRF5 activation leads to macrophage migration by upregulating PI3Kγ, which then promotes the formation of AAA. We highlight that disruption of the IRF5-PI3Kγ pathway in macrophages is an encouraging target for AAA treatment.

METHODS

Aortic Samples of AAA Patients

Human AAA specimens were harvested from patients who had undergone open AAA repair surgery, and normal aortas were collected from organ transplantation donors. All the procedures were followed the guidelines for the ethical treatment of human specimen and approved by Human Research Ethics Committee of the Second Affiliated Hospital, Zhejiang University School of Medicine. All participants gave written informed consent. The studies were conducted according to the Declaration of Helsinki principles.

Animals

All mice were males and C57BL/6 background. *Irf5*$^{-/-}$ and *Pik3cg*$^{-/-}$ mice were generated in GemPharmatech Co., Ltd. in Nanjing, China. We especially appreciate Dr. Jia Wei from Children's Hospital, Zhejiang University School of Medicine in Hangzhou, China, for providing *Irf5*$^{flox/flox}$ mice. *Irf5*$^{flox/flox}$ mice (stock no. 017311) were crossed to *Lyz2*^{Cre} mice (stock no. 004781), both from the Jackson Laboratory, to generate myeloid *Irf5* knockout mice (*Irf5*$^{\Delta M\Phi}$).

Irf5$^{flox/flox}$ mice was crossed to *Apoe*$^{-/-}$ mice (stock no.002052) to create *Irf5*$^{flox/flox}$ *Apoe*$^{-/-}$ mice. *Lyz2*^{Cre} mice were crossed to *Apoe*$^{-/-}$ mice, to generate *Lyz2*^{Cre} *Apoe*$^{-/-}$ mice. *Irf5*$^{flox/flox}$ *Apoe*$^{-/-}$ mice were crossed to *Lyz2*^{Cre} *Apoe*$^{-/-}$ mice, and *Irf5*$^{\Delta M\Phi}$ *Apoe*$^{-/-}$ mice were obtained. Using CRISPR/Cas9 technology, *Pik3cg* (*H11-CAG-LSL-Pik3cg-Flag-polyA*) was knocked in the *Irf5*$^{\Delta M\Phi}$ mice, to generate myeloid PI3Kγ overexpression mice at the background of *Irf5*$^{\Delta M\Phi}$ mice (*Pik3cg*$^{M\Phi+}$*Irf5*$^{\Delta M\Phi}$ mice) in GemPharmatech Co., Ltd.

AAA Induction in Mice

Elastase-induced AAA model was established as described previously in 10- to 12-week-old male mice(15). Briefly, the abdominal aorta between renal vein and iliac bifurcation was isolated, and all the aortic bifurcations were ligated. Subsequently, the aorta was temporary occluded proximally and distally, and an aortotomy was conducted by a 30-gauge needle. Heat-tapered polyethylene tubing (IN-10, ROBOZ) was introduced through aortotomy and secured with a tie. Type I porcine pancreatic elastase (Sigma) with 0.45 U/mL was perfused to aorta through tube for 15min at a constant pressure of 100 mmHg. The 100 mmHg was created by a saline bag hung at a height of 136 cm. Control mice were perfused with elastase inactivated at 100 ºC for 15 min. After the removal of the tubing, the aortotomy was closed with 11-0 suture. $CaPO_4$-induced mouse AAA model was conducted as previously reported(37). In 10- to 12-week-old male mice, isolated abdominal aorta was treated with small piece of gauze soaked in 0.5 mol/L $CaCl_2$ for 10 min, and replaced by

PBS-soaked gauze for 5 min. Control mice received PBS-soaked gauze for 15 min. Mice were terminated two weeks later, and the maximum external diameter of infrarenal aorta was measured before elastase or $CaPO_4$ administration (initial measurement) and at the time of sacrifice (final measurement). Aortic dilation was defined as aortic expansion relative to initial diameter ((Final measurement –initial measurement)/Initial measurement)*100, according to a previous report(15). Aortic tissues were embedded in optimal cutting temperature (OCT) Compound, and stored at -80 °C. Angiotensin-II (Ang-II)-induced AAA model was performed as previous studies(16,38). 10- to 12-week-old male mice were implanted with osmotic pumps(Alzet, model 2004) subcutaneously, and infused with saline or Ang-II (1000 ng/kg/min, Bachem) for continuous 28 days. After mice terminated, aortic tissues were fixed in 4% paraformaldehyde. Maximum abdominal aortic diameters were measured by photos taken from aortic tissues. If mice died before terminated at 28 days, Necropsies was performed to validate rupture, and the ruptured mice were only used for the calculation of mortality. All animal experiments were approved by the Animal Ethical Committee of the Second Affiliated Hospital, Zhejiang University School of Medicine, in accordance with guidelines of the Institutional Animal Care and Use Committee at Zhejiang University College of Medicine.

Reagents

Antibodies aganist IRF5 antibodies(ab181553, ab2932), MMP-2(ab92536),

MMP-9(ab38898), FLAG(ab205606) were from Abcam. Antibodies aganist PI3Kγ (sc-166365), PCNA (Santa Cruz, sc-56) were purchased from Santa Cruz Biotechnology. CD68 antibody(MCA1957GA) and CD3 antibody(MCA1477GA) were from BioRad. Ly6G antibody(14-5931-82), MHC-II antibody(14-5321-82) and secondary antibodies(A-21208, A-21207, A-11005) were from Thermo Fisher Scientifc. APC anti-CD45 (103111), PE/Cy7 anti-CD11b (101215) and PE anti-F4/80 (123109) were purchased from Biolegend. CD31 antibody(550274) and V450 anti-Ly6C (560594) were from BD. α-SMA antibody(A2547) and PKH26 (PKH26PCL) were from Sigma. Recombinant murine TNF-α(315-01A) and murine M-CSF(315-02) protein were produced by PeproTech.

Histological Studies

Human aortic tissues were paraffin-embedded, cutting into 5μm thickness. All OCT-embedded samples were cut to 7μm. Van Gieson staining was conducted by Van Gieson kit (Sigma) as detailed by the manufacturer.Elastin degradation scores were evaluated as previously described (1,no elastin degradation or mild elastin degradation; 2, moderate; 3,moderate to severe; and 4, severe elastin degradation)(39). For immunostaining studies, paraffin-embedded sections were deparaffinized, rehydrated, and incubated in 10 mmol/L citrate buffer for antigen retrieval. Frozen sections were permeabilized with 0.1% TritonX for 20 minutes at room temperature. Using 5% bovine serum albumin (BSA), non-specific sites were blocked. Primary

antibodies and secondary antibodies were used, and nuclei were stained with DAPI. To validate the antibody specificity, tissues incubated with isotype antibody controls and secondary antibody only controls. Four high-power random fields per section. Three sections per sample were analyzed and quantified by Image-Pro Plus 6.0.

Isolation of Monocytes and Adoptive Monocyte Transfer

Bone marrow of femur and tibia from WT and *Irf5*$^{-/-}$ mice were flushed, and monocytes were isolated by Monocyte Isolation Kit (MACS, Miltenyi Biotec), as previously described(14). Briefly, obtained bone marrow cells were incubated with monocyte biotin-antibody and anti-biotin microbeads and subsequently washed and passed through magnetic columns. The unlabeled cells, representing enriched monocytes, were stained with PKH26 (10μM, Sigma). After elastase perfusion, each mouse was intravenously injected with PKH26 stained monocytes (10^6 cells) twice a week for two consecutive weeks. Aortic samples were harvested for further analysis.

Cell Culture and Transfections

Bone marrow-derived macrophages (BMDMs) were harvested as described previously(40). Briefly, bone marrow of femur and tibia was flushed, and cells were cultured in high glucose Dulbecco's modified Eagle's medium (DMEM) containing 10% FBS and mouse M-CSF recombinant protein (10 ng/ml, PeproTech) for 7 days. HEK293T cells, from ATCC, were cultured in high glucose DMEM medium supplemented with 10% FBS in a humidified

atmosphere of 5% CO_2 at 37 °C. Using lipofectamine RNAi MAX reagent (Invitrogen), scrambled (Scr) siRNA (Santa Cruz) or *Irf5* siRNA (Santa Cruz) was transfected into BMDMs at a confluence of 40%-60%, according to manufacturer's protocol.

Wound Healing and Transwell Migration Assays

The monolayer of BMDMs with 80-100% confluency was scratched by a sterile micropipette tip. The cells were washed by PBS, and fresh medium with TNF-α (50 ng/ml, PeproTech) was added. The images of wounded area were captured after scratch and 24 h later. The migratory abilities were assessed by counting total number of cells migration to the wounded areas, as previous reported(16). Transwell migration assays were performed in 24-well Transwell plates with 8 μm pore inserts. Macrophages (10^5 cells) were resuspended in 200 μl and seeded in the upper chamber. Medium with TNF-α (50 ng/ml, PeproTech) was placed in the lower chamber. After cell migration for 6 h, migratory cells in the lower surface of inserts were fixed and stained with DAPI. The number of migratory cells was quantified by fluorescence microscopy at 40X magnification.

Chromatin Immunoprecipitation Assay

Chromatin immunoprecipitation (ChIP) assay was performed with the SimpleChIP Enzymatic Chromatin IP Kit (9002, CST). All the procedures were in accord with the manufacturer's instructions. Briefly, 10^7 BMDMs were collected and lysed. Using micrococcal nuclease, DNA was digested into

150-900 bp fragments. The acquired chromatin was incubated with antibody against IRF5(ab2932) overnight at 4 °C, and subsequently was incubated with protein-G conjugated agarose beads for 2 h at 4 °C. All the DNA samples were purified. DNA was amplified by SYBR kits (Takara) on an Applied Biosystems 7500 Fast Real-Time PCR System (ABI). The primers used to amplify the binding regions (778-1083) were:

F: 5′-CCCCTAAACAATTCAAGCTACCC-3′,

R: 5′-CACGATGCACTGTACCCTCA-3′ (Core: TTGTAAAGATACCAA).

Luciferase Assay

For transfection of plasmids in HEK 293T, lipofectamine 3000 reagent (Invitrogen) was applied according to the manufacturer's protocol. The luciferase experiment includes 500 ng IRF5 plasmid, 500 ng mPik3cg promoter pGL3-Basic, and 40 ng pGL3-Basic-Renilla luciferase. Cellular extracts were harvested 48 hours after transfection and determined by dual-luciferase assay (Promega). Renilla activity was used as a normalization of firefly luciferase.

RNA Sequencing and Bioinformatic Analysis

Harvested tissues or cells were incubated in Trizol reagent (Invitrogen). Both RNA isolation and RNA-seq were performed by Novogene Co. Ltd (Headquarters). Briefly, RNA concentration was assessed by Qubit 2.0 Fluorometer (Life Technologies). The quality was verified by the Bioanalyzer 2100 system (Agilent Technologies). Libraries were created using NEBNext

564 UltraTM RNA Library Prep Kit for Illumina (NEB, USA) by manufacturer's
565 instructions. Clean reads were mapped to the mouse genome (GRCm38)
566 using STAR (v2.5.1b). featureCounts (v1.5.0) was used to count reads that
567 mapped to the entire gene body of genes(41). Differential gene expression
568 analysis was performed using DEseq2 (v1.20.0)(41). For adventitia tissue and
569 AAA tissues, genes with an FDR corrected *P*-value < 0.05 and log_2fold
570 change >1 (2-fold change) were considered statistically significant expression.
571 For BMDMs, genes with an FDR corroded *P*-value<0.05 and absolute log_2fold
572 change >0.26 (1.2-fold change) were considered significantly differential
573 expression. Pathway enrichment analysis of differentially expressed genes
574 was performed by Metascape. The list of transcription factors was referred to
575 online database (http://bioinfo.life.hust.edu.cn/static/AnimalTFDB3/download/
576 Mus_musculus_TF).

577 **Single-Cell RNA Analysis**

578 Database of single-cell RNA-seq of elastase-induced AAA referred to the
579 previous study(11). The reads of each library were processed separately using
580 the "cellranger count" pipeline to generate a gene-barcode matrix for each
581 library. Reads were aligned to the mouse (Mus musculus) reference genome
582 (version: mm10). The gene-cell barcode matrix was imported into Seurat
583 v3.2.2. To exclude poor quality cells that might result from multiplets or other
584 technical noise, we filtered cells that were considered outliers based on the
585 number of expressed genes detected (nCount_RNA less than 2500 & greater

than 18000), the sum of UMI counts (nFeature_RNA less than 300 & greater than 4000), the proportion of mitochondrial genes (greater than 10%), and the proportion of ribosome genes (greater than 40%). Then, we normalized the sum of UMI counts for each cell to the median of all cells. After normalization, the UMI count data were log-transformed.To mitigate the effects of uninteresting sources of variation, we regressed the effects of mitochondrial gene proportion, G2/M, and S scores with the “ScaleData” function. The ”CellCycleScoring” function in the Seurat package was used to assign each cell scores, i.e., G2/M and S scores, based on the expression of a panel of phase-specific marker genes. To reduce noise that may be introduced by considering all the genes, instead we selected 2000 highly variable genes (HVGs) that contribute greatly to cell-to-cell variation based on expression intensity and dispersion (the “FindVariableGenes” function). Then, the expression of the HVGs was used for linear dimensional reduction of the data through principal component analysis (PCA). Harmony package was used to remove batch effect among different samples. The first 20 principal components of PCA were used to cluster the cells through a graph-based unsupervised clustering approach implemented in Seurat (resolution = 0.8). Following clustering, all cells were projected onto a two-dimensional map by means of UMAP. Migration related genes were derived from enrichment analysis (GO:0050900, GO:0030335). The subpopulations in the single-cell data were merged, and the analysis of differential gene expression among

different cell types was performed. The genes with corrected *P*-value < 0.05 were regarded as macrophage highly expressed genes. Possible binding sites were defined as relative score > 0.8 by JASPAR prediction.

Flow Cytometry

Aortic tissues were harvested, cut into pieces, and digested into single-cell suspensions in Aorta Dissociation Enzyme Solution (ADES), as previously reported(42). The prepared single-cell suspensions were stained with antibodies for 30 min. 7-AAD was incubated in suspensions for 5 min before analysis. Cell isolates were washed, and the fluorescence was measured by flow cytometry with a BD FACS Canto II Flow Cytometer (BD Biosciences) and analyzed using FlowJo v10 (Tree Star). The gating strategy of macrophages was shown in Supplemental Figure 21. The population of singlets was gated on FSC-A/FSC-H dot plots. Leukocytes were defined as CD45 positive cells on SSC-A/CD45 dot plots. The population of macrophages was viewed as the $CD11b^{+}F4/80^{+}$ population in leukocytes, and monocytes was viewd as $CD11b^{+}Ly6C^{+}$ population.

Western Blot Analysis

Cells or aortic tissues were obtained and lysed by RIPA lysis buffer (RIPA, Beyotime) containing protease inhibitors. Protein concentration was evaluated by BCA assay (Invitrogen). Equal amounts of proteins were loaded onto each lane, separated by SDS-PAGE and transferred to PVDF membranes. Subsequently, the membranes were incubated with primary antibodies at 4°C

overnight and secondary antibodies for 1 h. The bands were visualized by western blotting detection system including ChemiDoc MP (BioRad) and Amersham ImageQuant 800 (Cytiva). Data were normalized to the internal control.

Quantitative Real-time PCR

Total RNA was extracted from cells using Trizol reagent (Invitrogen). Generally, 500 ng of total RNA per sample was transcribed into cDNA by PrimeScript RT reagent Kit (Takara). The acquired cDNA was amplified by SYBR kits (Takara) on an Applied Biosystems 7500 Fast Real-Time PCR System (ABI). *Actb* was used as an internal control.

Statistical Analysis

All values are presented as mean ± s.d of at least three independent experimental repeats. Unpaired two-tailed Student's *t*-test was used to evaluate statistical differences between two groups, while ANOVA with Bonferroni multiple comparisons were applied for three or more groups. For variable that were not continuous, Mann Whitney test was applied for two groups. P value less than 0.05 was considered statistically significant. Statistical calculations were performed using GraphPad Prism 8.0.

Study approval

All the procedures of human samples acquirement were followed the guidelines for the ethical treatment of human specimen and approved by Human Research Ethics Committee of the Second Affiliated Hospital, Zhejiang

University School of Medicine (2019-401). All participants gave written informed consent. The studies were conducted according to the Declaration of Helsinki principles. All procedures of animal experiments were in accordance with guidelines of the Institutional Animal Care and Use Committee at Zhejiang University College of Medicine.

Data availability.

The authors declare that the data that support the findings of this study are available from the corresponding author upon reasonable request. Values for all data points in graphs are listed in the Supporting Data Values file. Raw RNA-seq data were submitted to NCBI-SRA. The BioProject accession number were PRJNA817520, PRJNA817410 and PRJNA855153.

Author contributions

YW conducted experiments, acquired data, analyzed data, performed statistical analysis, and wrote the manuscript. ZL harvested human samples, conducted experiments and acquired data. SS performed all the bioinformatic analysis. JW, LJ, YM and TY conducted animal experiments. CJ conducted animal experiments and obtained funding for the study. ZC and MX supervised all the study and obtained funding for the study. All authors discussed and revised the manuscript, and approved the final version of the manuscript.

Acknowledgments

This work was supported by the National Natural Science Foundation of China (81870203 to MX, 81970396 to ZC, 81700412 to CJ, 82100500 to YW).

References

1.Sakalihasan N, et al. Abdominal aortic aneurysms. *Nat Rev Dis Primers.* 2018; 4(1): 34.

2.Zhao Y, et al. Changes in cardiovascular disease burden in China after release of the 2011 Chinese guidelines for cardiovascular disease prevention: a bayesian causal impact analysis. *Cardiovasc Innov Appl*.2023;8(1):53.

3.Nordon IM,et al. Pathophysiology and epidemiology of abdominal aortic aneurysms. *Nat Rev Cardiol.* 2011; 8(2): 92-102.

4.Wang YD, et al. Pharmacological therapy of abdominal aortic aneurysm: an update. *Curr Vasc Pharmacol*. 2018;16(2):114-124.

5.Raffort J, et al. Monocytes and macrophages in abdominal aortic aneurysm. *Nat Rev Cardiol.* 2017; 14(8): 457-471.

6.Dale MA, et al. Inflammatory cell phenotypes in AAAs: their role and potential as targets for therapy. *Arterioscler Thromb Vasc Biol.* 2015; 35(8): 1746-1755.

7.Zhao GN, et al. Interferon regulatory factors: at the crossroads of immunity, metabolism, and disease. *BBA-Mol Basis Dis.* 2015; 1852(2):365-378.

8.Kaur A, et al. IRF5-mediated immune responses and its implications in immunological disorders. *Int Rev Immunol.*2018; 37(5):229-248.

9.Liu Z, et al. Hyperhomocysteinemia exaggerates adventitial inflammation and angiotensin II−induced abdominal aortic aneurysm in mice. *Circ Res.* 2012;111(10):1261-1273.

10.Stenmark KR, et al. The adventitia: essential regulator of vascular wall structure and function. *Annu Rev Physiol.* 2013; 75:23-47.

11.Zhao G, et al. Single-cell RNA sequencing reveals the cellular heterogeneity of aneurysmal infrarenal abdominal aorta. *Cardiovasc Res.* 2021;117(5):1402-1416.

12.Lysgaard Poulsen J, et al. Animal models used to explore abdominal aortic aneurysms: a systematic review. *Eur J Vasc Endovasc Surg*. 2016;52(4):487-499.

13.Sénémaud J, et al. Translational relevance and recent advances of animal models of abdominal aortic aneurysm. *Arterioscler Thromb Vasc Biol.* 2017;37(3):401-410.

14.de Souza VCA, et al. Adoptive transfer of bone marrow-derived monocytes ameliorates Schistosoma mansoni-induced liver fibrosis in mice. *Sci Rep*.2019;9(1):6434.

15.Liu Z, et al. Thrombospondin-1 (TSP1) contributes to the development of vascular inflammation by regulating monocytic cell motility in mouse models of abdominal aortic aneurysm. *Circ Res.* 2015; 117(2):129-141.

16.Ma D, et al. Inhibition of KLF5-Myo9b-RhoA pathway-mediated podosome formation in macrophages ameliorates abdominal aortic aneurysm.*Circ Res.* 2017; 120(5):799-815.

17.Patel J, et al. RGS1 regulates myeloid cell accumulation in atherosclerosis and aortic aneurysm rupture through altered chemokine signalling. *Nat*

719 *Commun.*2015; 6: 6614.

720 18.Liu R, et al. Inhibition of phosphatidylinositol 3-kinase γ by IPI-549
721 attenuates abdominal aortic aneurysm formation in mice. *Eur J Vasc Endovasc*
722 *Surg*. 2020;60(2):254-263.

723 19.Ensan S, et al. Self-renewing resident arterial macrophages arise from
724 embryonic CX3CR1^{+} precursors and circulating monocytes immediately after
725 birth. *Nat Immunol.* 2016; 17(2): 159-168.

726 20.Krausgruber T, et al. IRF5 promotes inflammatory macrophage polarization
727 and TH1-TH17 responses. *Nat Immunol.*2011; 12(3): 231-238.

728 21.Dalmas E, et al. Irf5 deficiency in macrophages promotes beneficial
729 adipose tissue expansion and insulin sensitivity during obesity. *Nat Med.* 2015;
730 21(6): 610-618.

731 22.Wei J, et al. Irf5 deficiency in myeloid cells prevents necrotizing
732 enterocolitis by inhibiting M1 macrophage polarization. *Mucosal Immunol.*
733 2019; 12(4): 888-896.

734 23.Khoyratty TE, et al. Diverse mechanisms of IRF5 action in inflammatory
735 responses. *Int J Biochem Cel Biol.*2018; 99: 38-42.

736 24.Kaur A, et al. IRF5-mediated immune responses and its implications in
737 immunological disorders. *Int Rev Immunol.*2018; 37(5):229-248.

738 25.Seneviratne AN, et al. Interferon regulatory factor 5 controls necrotic core
739 formation in atherosclerotic lesions by impairing efferocytosis. *Circulation.*
740 2017; 136(12): 1140-1154.

741 26.Edsfeldt A, et al. Interferon regulatory factor-5-dependent CD11c+
742 macrophages contribute to the formation of rupture-prone atherosclerotic
743 plaques.*Eur Heart J*. 2022;43(19):1864-1877.
744 27.Orliaguet L, et al. Early macrophage response to obesity encompasses
745 Interferon Regulatory Factor 5 regulated mitochondrial architecture
746 remodelling.*Nat Commun*. 2022;13(1):5089.
747 28.Yang L, et al. Monocytes from Irf5-/- mice have an intrinsic defect in their
748 response to pristane-induced lupus. *J Immunol.* 2012;189(7): 3741-3750.
749 29.Hirsch E, et al. Central role for G protein-coupled phosphoinositide 3-kinase
750 gamma in inflammation. *Science.* 2000; 287(5455): 1049-1053.
751 30.Barberis L, et al. Leukocyte transmigration is modulated by
752 chemokine-mediated PI3Kγ-dependent phosphorylation of vimentin. *Eur J*
753 *Immunol.*2009; 39(4): 1136-1146.
754 31.Hawkins PT, et al. PI3K signalling in inflammation. *Biochim Biophys Acta.*
755 2015; 1851(6): 882-897.
756 32.Fougerat A, et al. Genetic and pharmacological targeting of
757 phosphoinositide 3-kinase-gamma reduces atherosclerosis and favors plaque
758 stability by modulating inflammatory processes. *Circulation.* 2008; 117(10):
759 1310-1317.
760 33.Yu J, et al. Inhibition of Phosphatidylinositol 3-kinease suppresses
761 formation and progression of experimental abdominal aortic aneurysms. *Sci*
762 *Rep.* 2017; 7(1): 15208.

763 34.Smirnova NF, et al. Targeting PI3Kγ activity decreases vascular
764 trauma-induced intimal hyperplasia through modulation of the Th1 response. *J*
765 *Exp Med.* 2014; 211(9): 1779-1792.
766 35.Courties G, et al. In vivo silencing of the transcription factor IRF5
767 reprograms the macrophage phenotype and improves infarct healing.*J Am*
768 *Coll Cardiol*. 2014;63(15):1556-1566.
769 36.Zhang M, et al. Myeloid HO-1 modulates macrophage polarization and
770 protects against ischemia-reperfusion injury. *JCI Insight*. 2018;3(19):e120596.
771 37.Yamanouchi D, et al. Accelerated aneurysmal dilation associated with
772 apoptosis and inflammation in a newly developed calcium phosphate rodent
773 abdominal aortic aneurysm model. *J Vasc Surg.* 2012; 56(2): 455-461.
774 38.Vandestienne M, et al. TREM-1 orchestrates angiotensin II-induced
775 monocyte trafficking and promotes experimental abdominal aortic aneurysm.*J*
776 *Clin Invest.* 2021;131(2):e142468.
777 39.Morgan S, et al. Elevated protein kinase C-δ contributes to aneurysm
778 pathogenesis through stimulation of apoptosisand in fl ammatory signaling.
779 *Arterioscler Thromb Vasc Biol*. 2012;32(10):2493-2502.
780 40.Jia L, et al.Heme oxygenase-1 in macrophages drives septic cardiac
781 dysfunction via suppressing lysosomal degradation of inducible nitric oxide
782 synthase. *Circ Res.* 2018; 122(11): 1532-1544.
783 41.Liao Y, et al. featureCounts: an efficient general purpose program for
784 assigning sequence reads to genomic features. *Bioinformatics.* 2014; 30(7):

923-930.

42.Butcher MJ, et al. Flow cytometry analysis of immune cells within murine aortas. *J Vis Exp*. 2011; 53: 2848.

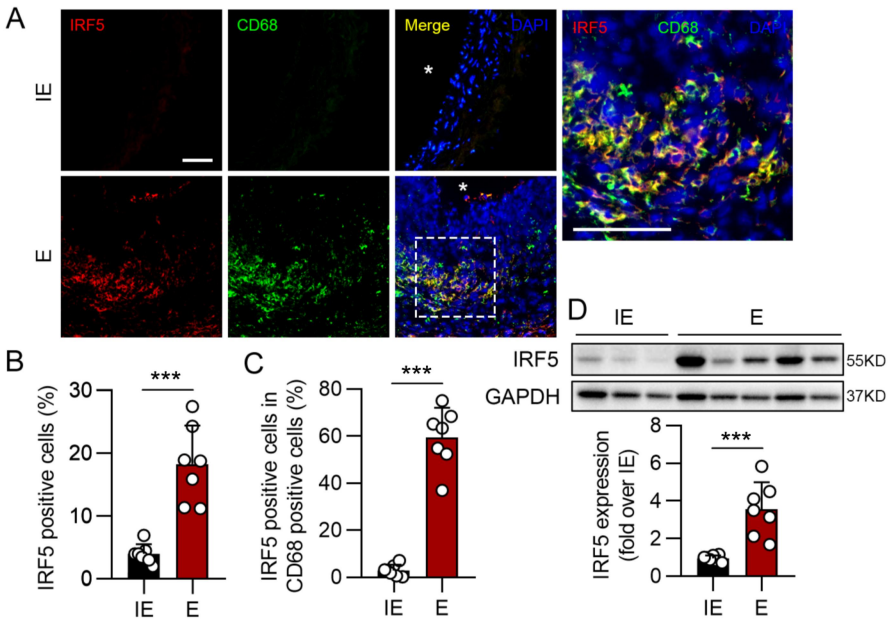

Figure 1. IRF5 is increased in elastase-induced AAA.

(**A**) Representative images of IRF5 and CD68 co-immunostaining in elastase-induced AAA samples. * indicates aortic lumen. Scale bar: 100 μm. (**B** and **C**)Quantification of IRF5 in mice treated with inactive elastase (IE, n = 7) and elastase (E, n = 7). (**D**) Western blot analysis revealed that IRF5 expression in elastase-induced AAA tissues was dramatically increased compared to the IE group. Data in (**B-D**) are presented as mean ± s.d, and significance is determined by unpaired two-tailed Student's *t*-test (***$P < 0.001$).

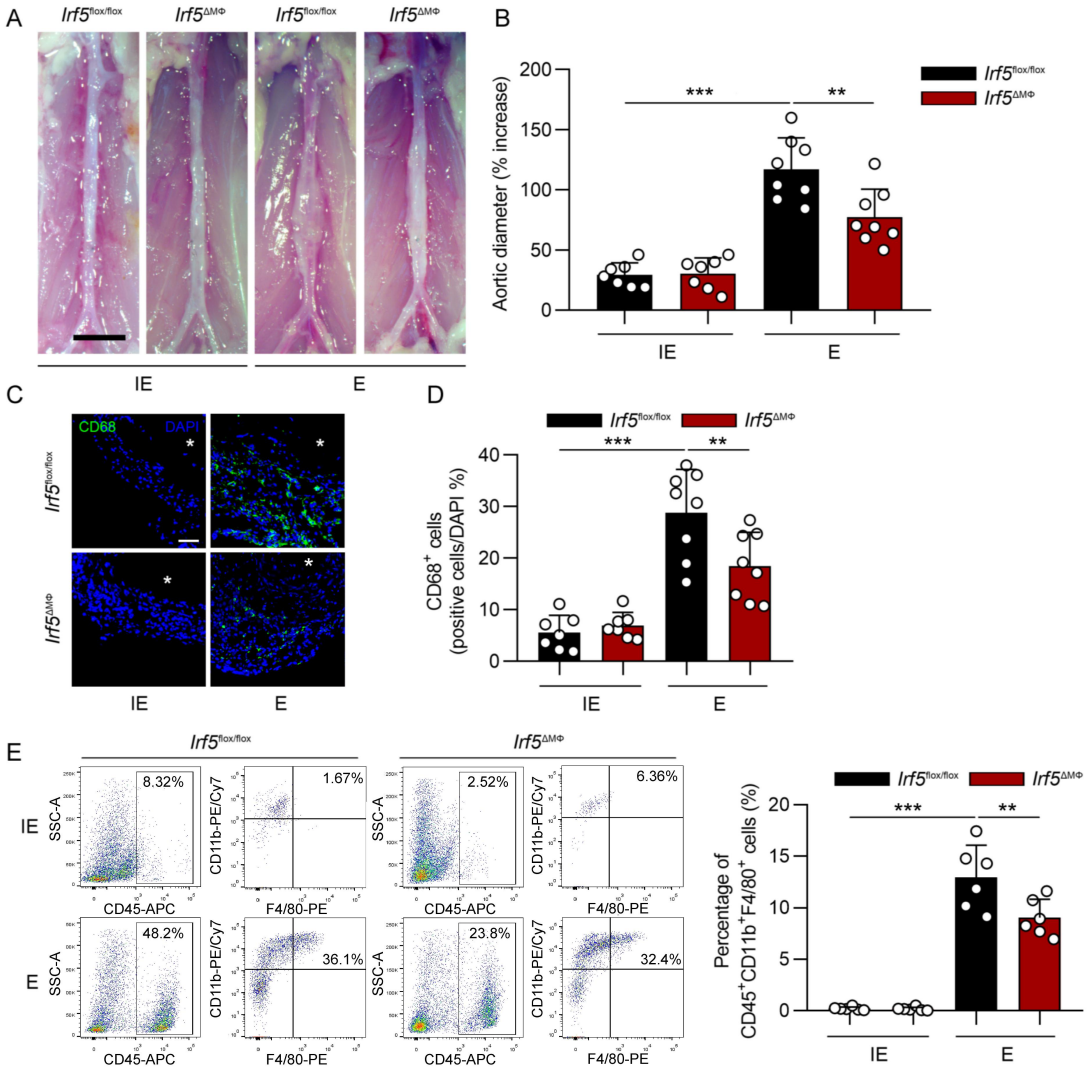

Figure 2. Myeloid cell-specific *Irf5* deletion attenuates elastase-induced AAA and macrophage infiltration.

(**A** and **B**) Representative images of *Irf5*$^{flox/flox}$ and *Irf5*$^{\Delta M\Phi}$ infra-renal abdominal aortas 14 days after treatment of inactive elastase (IE) or elastase (E). The *Irf5*$^{flox/flox}$ mice perfused with elastase showed significant aortic dilation compared to that with IE perfusion. Myeloid cell-specific ablation of *Irf5* markedly decreased aortic dilation compared to that in *Irf5*$^{\Delta M\Phi}$ mice with elastase treatment. (n = 7 in the *Irf5*$^{flox/flox}$ mice with IE; n = 7 in *Irf5*$^{\Delta M\Phi}$ mice with IE; n = 8 in the *Irf5*$^{flox/flox}$ with E; n = 8 in the *Irf5*$^{\Delta M\Phi}$ with E) Scale bar: 2 mm. (**C** and **D**) Representative images of immunofluorescence staining of CD68 in AAA tissues from *Irf5*$^{flox/flox}$ and *Irf5*$^{\Delta M\Phi}$ mice treated with IE or E for two weeks. The quantitative analysis of CD68 staining was present at right. * indicates aortic lumen. Scale bar: 100 μm. (**E**) Representative flow cytometric analysis of macrophages ($CD45^+CD11b^+F4/80^+$) in

abdominal aortas of *Irf5*$^{flox/flox}$ and *Irf5*$^{\Delta M\Phi}$ mice followed by IE or E perfusion for two weeks (n = 6 in each group). Quantification of macrophages by flow cytometry was shown at right. Data in (**B, D** and **E**) are presented as mean ± s.d, and the significance is determined by two-way ANOVA followed by Bonferroni test ($^{**}P < 0.01$, $^{***}P < 0.001$).

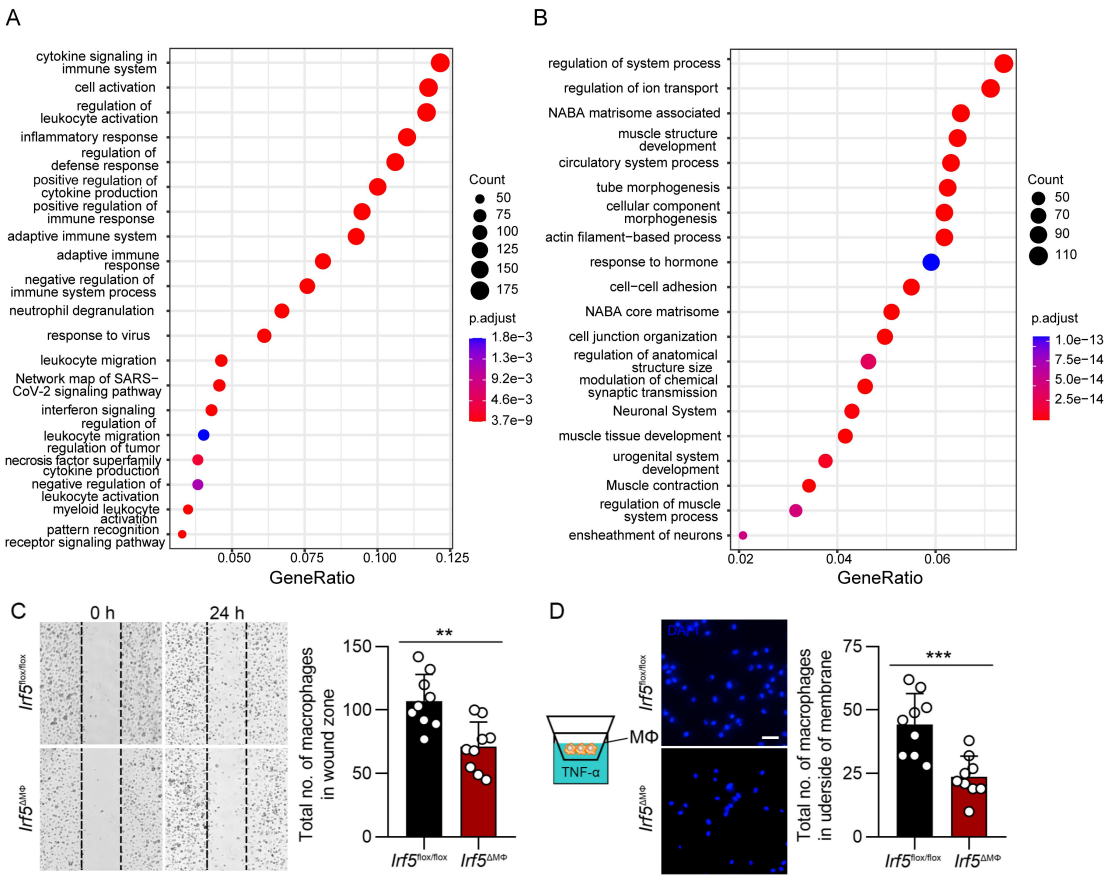

Figure 3. IRF5 contributes to macrophage migration.

(**A** and **B**) Dotplot represents enrichment analysis of genes corresponding to the down-regulated and up-regulated differentially expressed genes, respectively, between *Irf5*$^{-/-}$ AAA tissues and WT AAA tissues. Enrichment analysis was performed with metascape with a cutoff *P*-adjusted adjusted < 0.05 and $\log_2$fold change >1. The top 20 gene ontologies were listed. (**C**) Representative pictures of wound healing assays conducted with macrophages from *Irf5*$^{flox/flox}$ and *Irf5*$^{\Delta M\Phi}$ mice immediately after scratching and 24 h later (n = 9). Cells migrating to wound zone were quantified. (**D**) A transwell system was shown that macrophages were seeded in the upper chamber, and medium with TNF-α was placed in the lower chamber. Cells transmigrating through the filter to the underside of membranes were stained with DAPI and quantified (n = 9). Scale bar: 50 μm. Data in (**C** and **D**) are presented as mean ± s.d, and significance is determined by unpaired two-tailed Student's *t*-test ($^{**}P < 0.01$, $^{***}P < 0.001$).

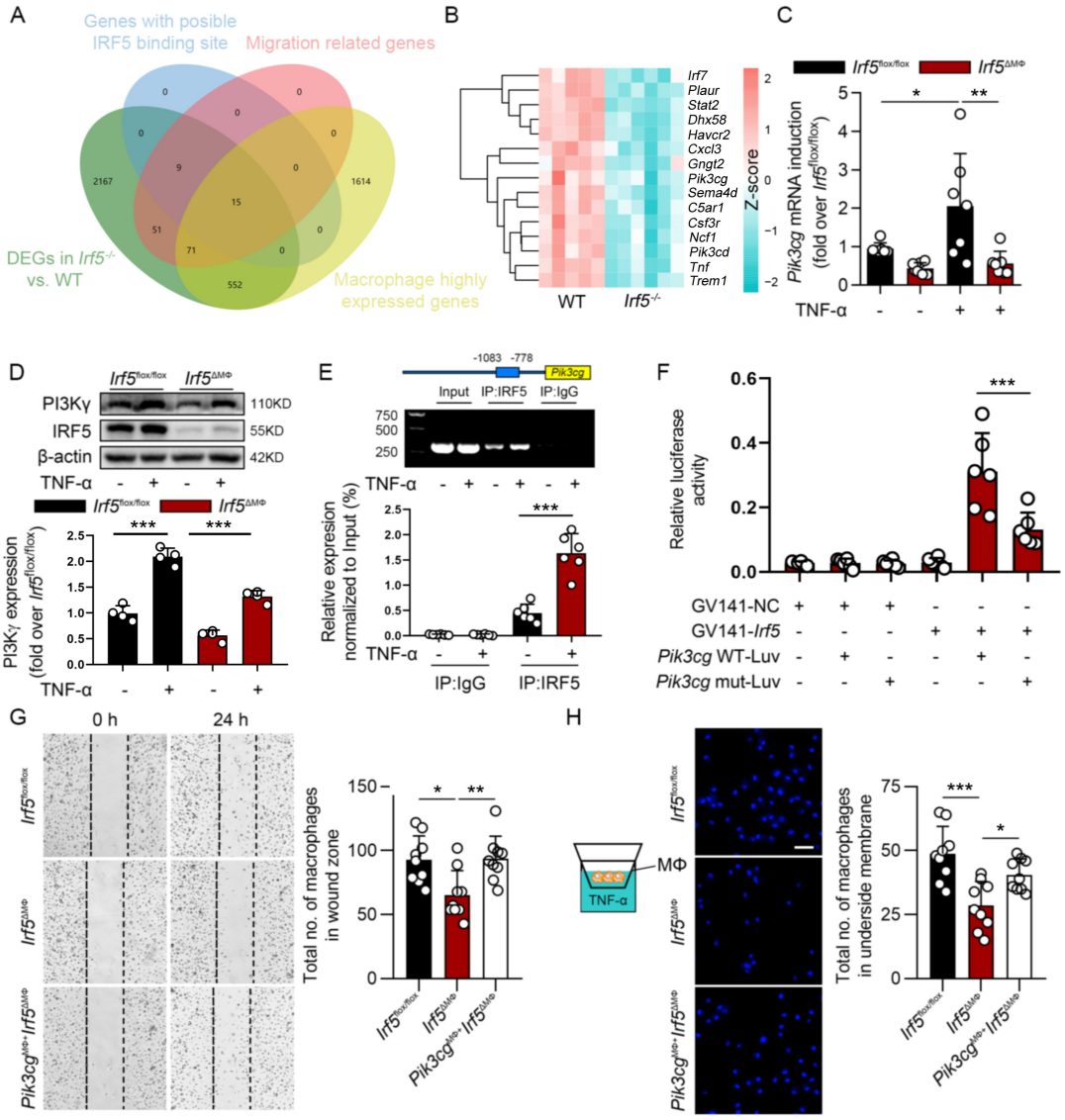

Figure 4. IRF5 promotes macrophage migration via PI3Kγ.

(**A**) Venn diagram based on the overlapping genes among differentially expressed genes (DEGs), migration related genes, macrophage highly expressed genes, and genes with potential IRF5 binding site. (**B**) Heat map of the 15 overlapping genes in AAA tissues from WT and *Irf5*$^{-/-}$ mice. (**C** and **D**) Macrophages from *Irf5*$^{flox/flox}$ and *Irf5*$^{\Delta M\Phi}$ mice were treated or not with TNF-α (50 ng/ml). The mRNA (n = 7)and protein (n = 4) levels of PI3Kγ were decreased in macrophages with IRF5 deletion. (**E**) Bone marrow-derived macrophages (BMDMs) stimulated with TNF-α (50 ng/ml) or not for 2 h were collected, and chromatin immunoprecipitation assays were conducted (n = 6). Chromatin was immunoprecipitated and assessed by PCR analysis to determine the binding site on *Pik3cg* promoter. (**F**) Dual-luciferase assays indicated that *Irf5* expression plasmid transfected into 293T cells

856 increased luciferase activity of *Pik3cg* promoter-reporter plasmids, and luciferase activity
857 was reduced when *Pik3cg* promoter-reporter plasmids contained -1060 to -1047 deletion
858 (n = 6). (**G** and **H**) Migration abilities of macrophages from *Irf5*$^{flox/flox}$, *Irf5*$^{\Delta M\Phi}$ and
859 *Pik3cg*$^{M\Phi+}$*Irf5*$^{\Delta M\Phi}$ mice were measured by wound healing and transwell assays (n = 9).
860 Excessive PI3Kγ expression promoted macrophage migration. Scale bar: 50 μm. Data are
861 presented as mean ± s.d, and the significance is determined by two-way ANOVA followed
862 by Bonferroni test in (**C-E**) and one-way ANOVA followed by Bonferroni test in (**F-H)** (**P* <
863 0.05, ***P* < 0.01, ****P* < 0.001).
864
865
866
867

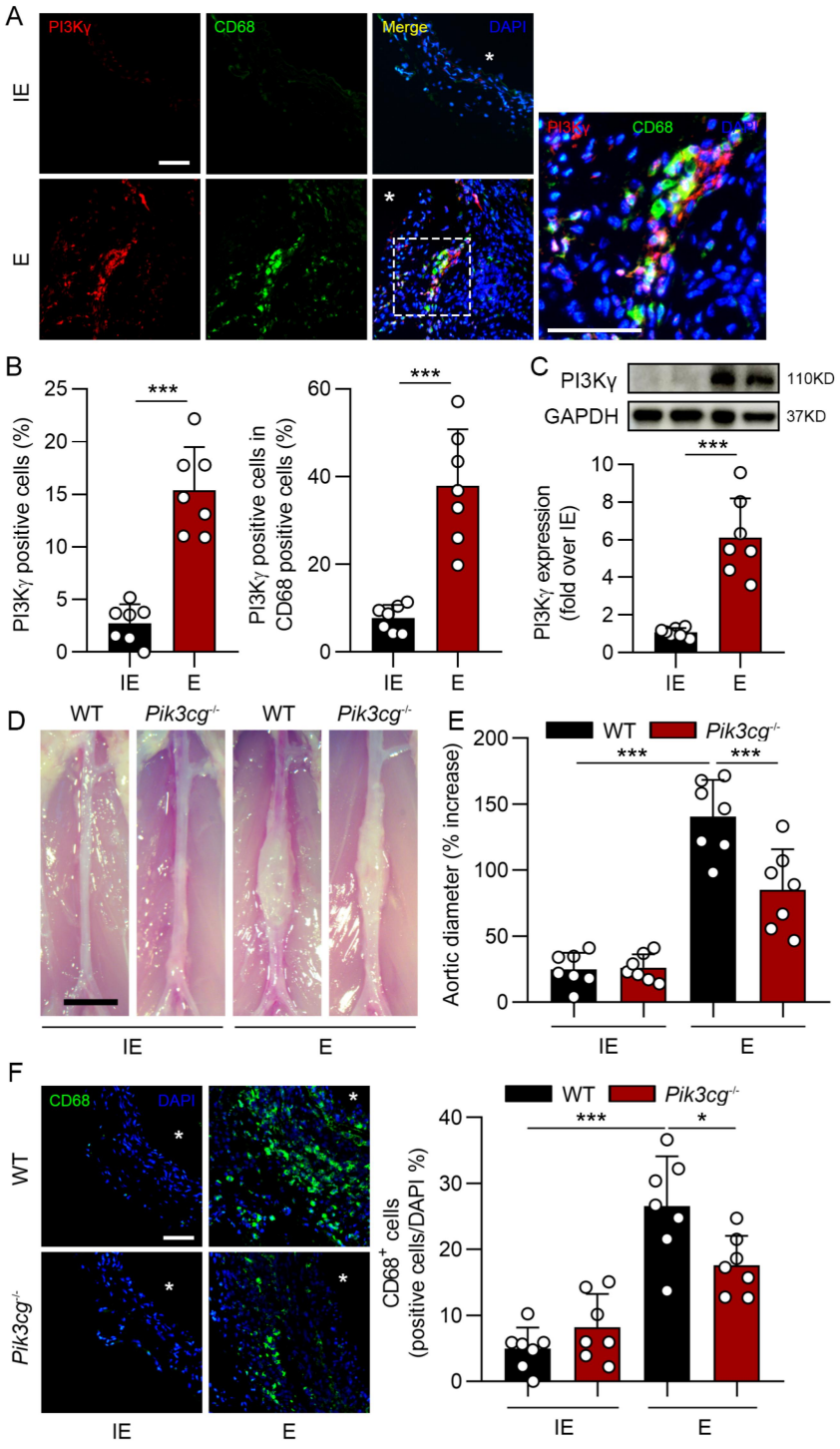

Figure 5. *Pik3cg* deficiency hinders elastase-induced AAA dilation.

(**A** and **B**) Representative images of immunofluorescence staining of PI3Kγ and CD68 in elastase-induced AAA from wild type mice. Quantification of PI3Kγ in mice treated with inactive elastase (IE, n = 7) or elastase (E, n = 7). * indicates aortic lumen. Scale bar: 100 μm. (**C**) Western blot analysis suggested that PI3Kγ expression in elastase-induced AAA tissues was significantly increased compared to the IE group. (**D** and **E**) Representative

875 photographs of WT mice and *Pik3cg*$^{-/-}$ mice subjected to IE or E treatment. *Pik3cg*$^{-/-}$ mice
876 showed a reduced AAA expansion compared to that of wild type mice. (n = 7 in the WT
877 mice with IE; n = 7 in *Pik3cg*$^{-/-}$ mice with IE; n = 7 in the WT with E; n = 7 in the *Pik3cg*$^{-/-}$
878 with E). Scale bar: 2 mm. (**F**) CD68 immunostaining in AAA tissues from WT mice and
879 *Pik3cg*$^{-/-}$ mice after elastase treatment for two weeks. Quantification was shown at right. *
880 indicates aortic lumen. Scale bar: 100 μm. Data are presented as mean ± s.d, and the
881 significance is determined by unpaired two-tailed Student's *t*-test in (**B** and **C**) and
882 two-way ANOVA followed by Bonferroni test in (**E** and **F**) ($*P < 0.05$, $***P < 0.001$).
883

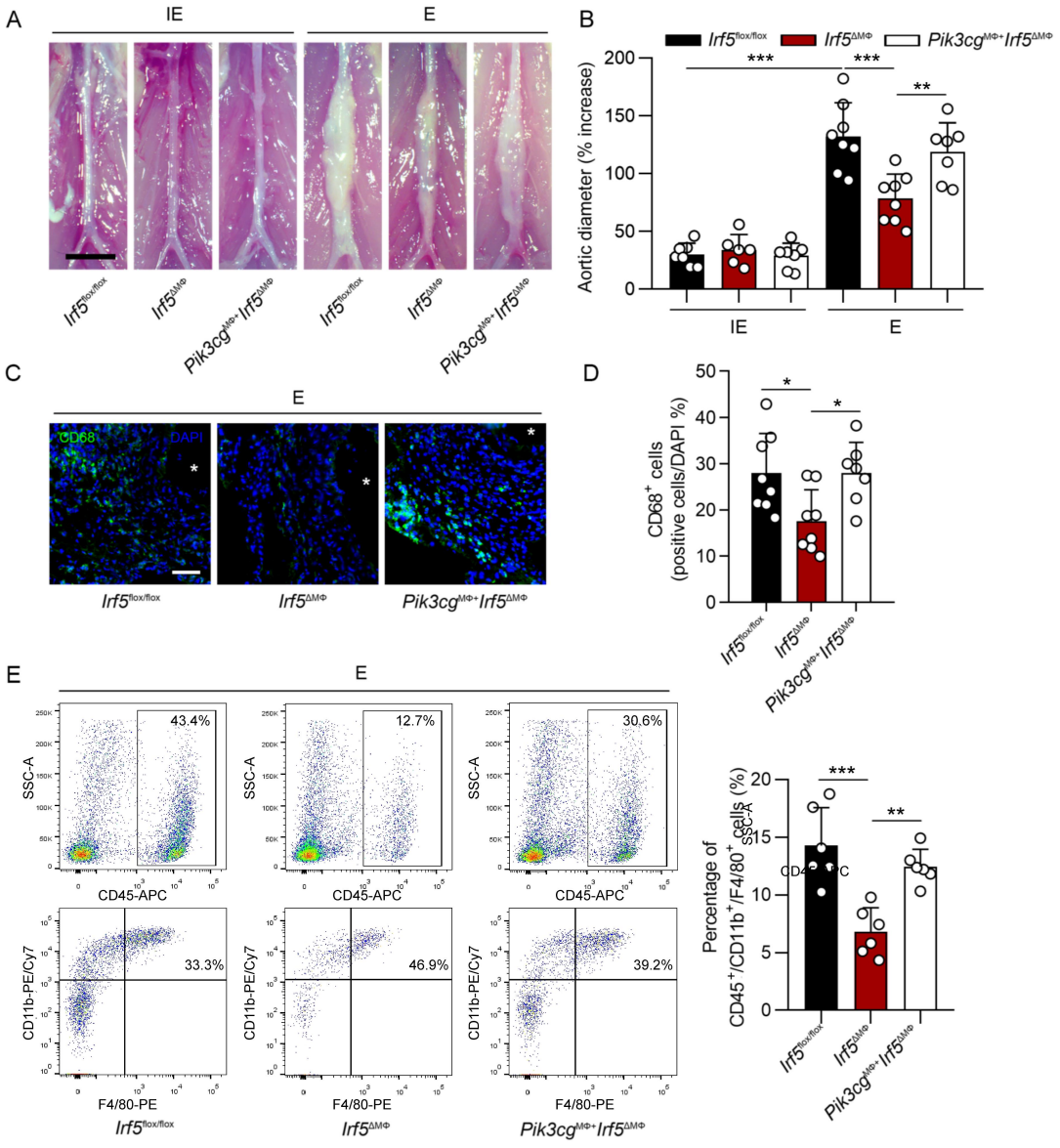

Figure 6. Myeloid cell-specific salvage of *Pik3cg* restores *Irf5* ablation-induced AAA reduction.

(**A** and **B**) Representative photos of *Irf5*$^{flox/flox}$, *Irf5*$^{\Delta M\Phi}$ and *Pik3cg*$^{M\Phi+}$*Irf5*$^{\Delta M\Phi}$ mice infra-renal abdominal aortas followed by elastase (E) or inactive elastase (IE) perfusion. *Pik3cg* overexpression in myeloid cells dramatically increased aortic dilation compared to that with *Irf5*$^{\Delta M\Phi}$ mice. (n = 7 in the *Irf5*$^{flox/flox}$ mice with IE; n = 6 in *Irf5*$^{\Delta M\Phi}$ mice with IE; n = 7 in the *Pik3cg*$^{M\Phi+}$*Irf5*$^{\Delta M\Phi}$ mice with IE; n = 8 in the *Irf5*$^{flox/flox}$ with E; n = 8 in the *Irf5*$^{\Delta M\Phi}$ with E; n = 7 in the *Pik3cg*$^{M\Phi+}$*Irf5*$^{\Delta M\Phi}$ mice with E). Scale bar: 2 mm. (**C** and **D**) Representative images of CD68 immunostaining in AAA tissues from *Irf5*$^{flox/flox}$, *Irf5*$^{\Delta M\Phi}$ and *Pik3cg*$^{M\Phi+}$*Irf5*$^{\Delta M\Phi}$ mice after elastase treatment for two weeks. The CD68 staining was

quantified. * indicates aortic lumen. Scale bar: 100 μm. (**E**) Representative flow cytometric analysis of macrophages ($CD45^+CD11b^+F4/80^+$) in aortas of *Irf5*$^{flox/flox}$, *Irf5*$^{\Delta M\Phi}$ and *Pik3cg*$^{M\Phi+}$*Irf5*$^{\Delta M\Phi}$ mice with AAA establishment (n = 6 in each group). Quantification of macrophages by flow cytometry was shown at the right. Data are presented as mean ± s.d, and the significance is determined by two-way ANOVA followed by Bonferroni test in (**B**) and one-way ANOVA followed by Bonferroni test in (**D** and **E**) (**P* < 0.05, ***P* < 0.01, ****P* < 0.001).

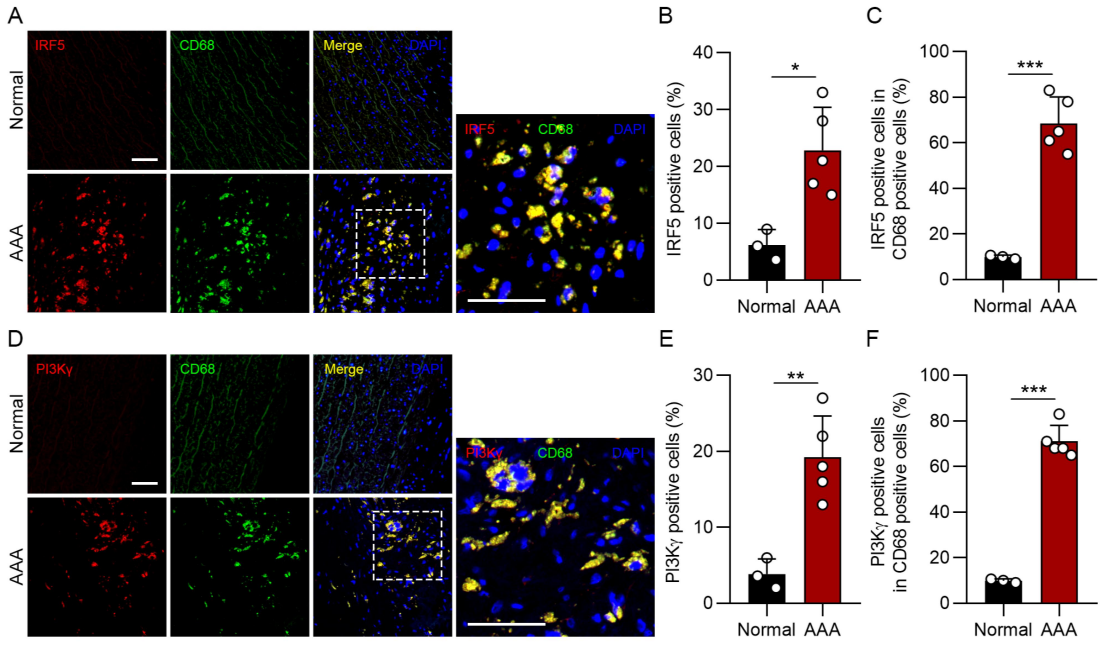

Figure 7. IRF5 and PI3Kγ are induced in infiltrated macrophages in human AAA. (**A-C**) Representative images of immunofluorescence staining of IRF5 and CD68 in human AAA tissues. In AAA tissues, IRF5 was mostly located in the aortas and presented in infiltrated CD68-positive cells. Quantification of IRF5 in normal aortas (n = 3) and AAA samples (n = 5) was shown at right. (**D-F**) Representative images of immunofluorescence staining of PI3Kγ and CD68 in human AAA tissues. PI3Kγ was highly expressed in macrophages of human AAA samples. Quantification of PI3Kγ in normal aortas (n = 3) and AAA samples (n = 5) was shown at right. Scale bar: 100 μm. Data in (**B, C, E** and **F)** are presented as mean ± s.d, and the significance is determined by unpaired two-tailed Student's *t*-test ($*P < 0.05$, $**P < 0.01$, $***P < 0.001$).